

pubs.acs.org/cm Article

# Donor—Acceptor Conjugated Copolymers Containing Transition-Metal Complex: Intrachain Magnetic Exchange Interactions and Magneto-Optical Activity

Xunshan Liu, $^{*,\perp}$  Jiaze Xie, $^{\perp}$  Jens Niklas, Emigdio E. Turner, Dafei Yuan, John S. Anderson, Jeffrey J. Rack, Oleg G. Poluektov, and Luping Yu\*



Cite This: Chem. Mater. 2022, 34, 5740-5747



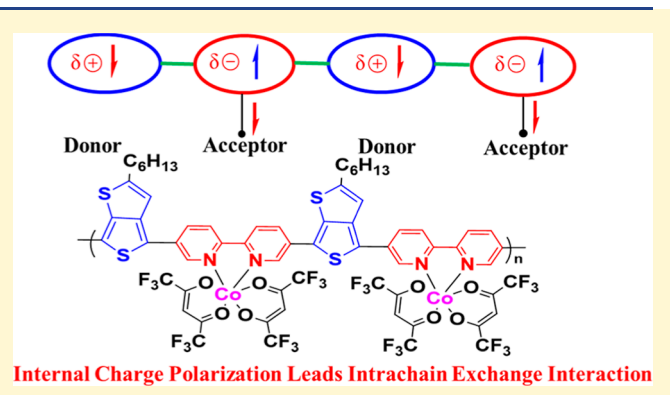
**ACCESS** I

III Metrics & More

Article Recommendations

Supporting Information

ABSTRACT: A donor—acceptor conjugated copolymer containing thienothiophene (donor) units and Co(II) complexes (acceptor) has been synthesized and characterized. The studies of magnetic properties of the polymers by SQUID and EPR measurements showed antiferromagnetic exchange interaction between neighboring spin centers along with the polymer backbone through intrachain interactions. It is the first time that the D–A conjugated polymer backbone serves as bridging ligands for magnetic couplings, making these type of polymers promising as magnetic materials. Moreover, the magneto-optical activity of polymer LCP1 was characterized using magnetic circular dichroism spectroscopy. It was found that the material exhibits a large magneto-optic rotation with a peak Verdet constant of 2980 deg·T<sup>-1</sup>·m<sup>-1</sup> at 590 nm.



#### ■ INTRODUCTION

Organic semiconducting polymers exhibit multifunctions that can be utilized in many applications, such as optical, thermal, electrical, and stretchable electronic devices. <sup>1–4</sup> However, the ferromagnetism of pure organic polymers is still a challenging target to achieve. In contrast, many coordination complexes exhibit diverse magnetic behaviors such as single molecular magnet, spin crossover, long-term magnetic ordering, and spin frustration. <sup>5–8</sup> The incorporation of transition-metal complexes into conjugated polymer ligands combines the advantages of these two classes of materials and adds a new dimension of designing novel properties, such as mechanical flexibility, solubility, biocompatibility, (anti)ferromagnetic properties, and magneto-optical activity (MOA). <sup>9–12</sup>

To gain strong spin—spin interactions and stable magnetic properties, one needs to improve the orbital overlaps or introduce unpaired electrons. The magnetic properties of metal complexes are influenced by the strength of the ligand field, namely, the surrounding chemical environments of the spin centers. The spin-exchange interaction will be affected mainly by the properties of the bridges between the magnetic centers, such as size, polarity, and electronic properties. Essentially, the electronic properties of the coupling unit play the key role in mediating the spin—spin interactions. Polarized coupling units induce partial spin characters to enhance the spin interactions between the connected magnetic centers. 18,19,23 Conjugated D—A systems were shown to exhibit

spin characters due to the polarization.<sup>24</sup> However, coupling interactions due to magnetic exchange through conjugated D—A polymeric ligands are not well studied.

Our group previously developed conjugated polymers containing transition-metal complexes chelated onto the polymer backbones. Those polymers show interesting photoconductive and photorefractive properties.<sup>25–28</sup> Those polymers containing first row transition-metal complexes barely exhibited intrachain spin-spin interaction.<sup>28</sup> The d-electron spin state in the polymer complexes is the same as that of their corresponding monomers. The weak spin-spin interaction is most probably due to large separation between the magnetic centers. It was also found that the spins have not been quenched by the polymerization process, indicating the possibility to further modify the polymer structures to enhance the intrachain spin-spin coupling and to develop processible magneto-optic materials. 10,12 These results inspired us to further develop a suitable conjugated polymer backbone that can be used as a polymer ligand, in which the spin-spin

Received: May 12, 2022 Revised: June 4, 2022 Published: June 16, 2022





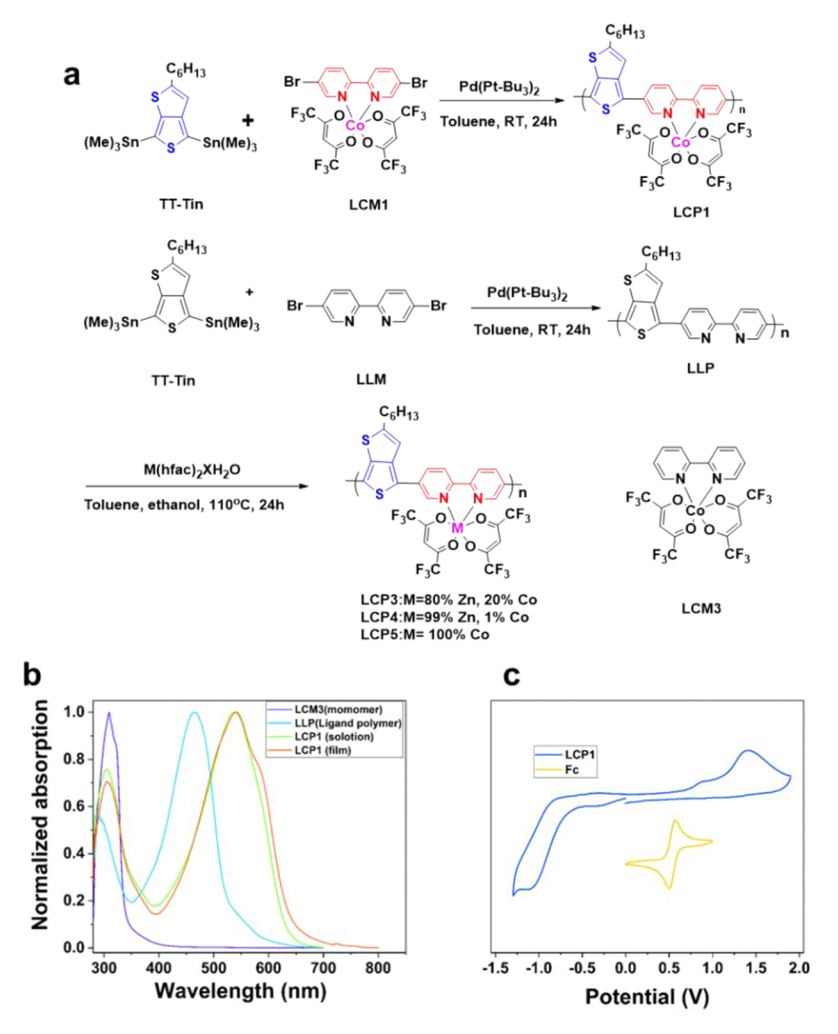


Figure 1. (a) Structures and synthetic routes of donor—acceptor complex copolymers LCPn and their corresponding metal complex ratios (feeding ratios). (b) Normalized UV—vis absorption spectra of the complex monomer unit (LCM1), ligand polymer (LLP), and complex polymer (LCP1) in CHCl<sub>3</sub>. (c) CV curve of LCP1 film in acetonitrile solution (0.1 M Bu<sub>4</sub>NPF<sub>6</sub>, as electrolyte) at room temperature (vs Fc/Fc<sup>+</sup>).

distance is shortened and the spin exchange interactions are strengthened along the polymer backbones.

This paper describes the synthesis of a series of D-A copolymers (LCPn) comprised of cobalt complexes and thienothiophene (TT) donor units. The alkyl TT unit is an electron-rich moiety and designed as an electron donor unit, 29,30 and the small size of the TT unit shows the advantage to reduce the physical distance between the magnetic centers. Thus, the D-A character from the polymer backbone causes the intramolecular polarization between electron-rich TT units and the electron-deficient complex moiety, assisting in direct exchange coupling. Systematic electron paramagnetic resonance (EPR) and magnetic measurements, control experiments, and density functional theory (DFT) calculations showed that there are intrachain, antiferromagnetic interactions through the polymer backbones. Significant magneto-optical properties were observed by Faraday rotation spectroscopy. This work indicates a useful approach for developing conjugated magnetic polymer materials.

# ■ RESULTS AND DISCUSSION

Figure 1a shows the structures and the corresponding metal complex ratios of copolymers LCPn. Detailed synthetic

approaches of the monomers and polymers are described in Scheme S1 of the Supporting Information. The LCP1 appears purple in solid, obtained in a yield of 91% after Soxhlet extraction and reprecipitation of the chloroform fraction in methanol. The polymers exhibited excellent solubility in common organic solvents such as chloroform, THF, and chlorobenzene. The structures of the monomers and copolymers were confirmed by <sup>1</sup>H NMR, matrix-assisted laser desorption ionization time-of-flight (MALDI-TOF), inductively coupled plasma mass spectrometry (ICP-MS) (see data in Table S2), and elemental analysis. The metal contents and degrees of coordination of the copolymers were determined by ICP-MS. The degree of coordination in all of the polymers was as follows: about 85% Co for LCP1, 83% in total for LCP3 (67% Zn and 16% Co), 84% in total for LCP4 (83% Zn and 1% Co), and 87% Co for LCP5. The elemental percentages of C, H, N, and S were then calculated based on the degree of metalation. Since mixed metals exist in the copolymers LCP3 and LCP4, elemental analysis was not able to directly determine the degree of coordination, and the results were in good agreement with the calculated elemental components based on ICP-MS measurements. Detailed data are listed in the synthesis part in the Supporting Information. The high coordination yields ( $\sim$ 85%) ensured the existence of

Table 1. Optical and Electrochemical Properties of the Polymer LCP1

	solution $\lambda_{s,max}$ (nm) <sup>a</sup>	film $\lambda_{f,max}$ (nm)	film $\lambda_{edge}$ (nm)				
copolymer	Abs.	Abs.	Abs.	$E_{\rm g}^{\rm opt} ({\rm eV})^{b}$	HOMO (eV)	LUMO (eV)	$E_{\rm g}^{\rm \ ec}$ (eV)
LCP1	538	542	671	1.85	-5.00	-3.62	1.38
LLP	463				-5.45	-3.05	2.40

<sup>&</sup>lt;sup>a</sup>Measured in chloroform solution. <sup>b</sup>Band gap estimated from the optical absorption band edge of the films.

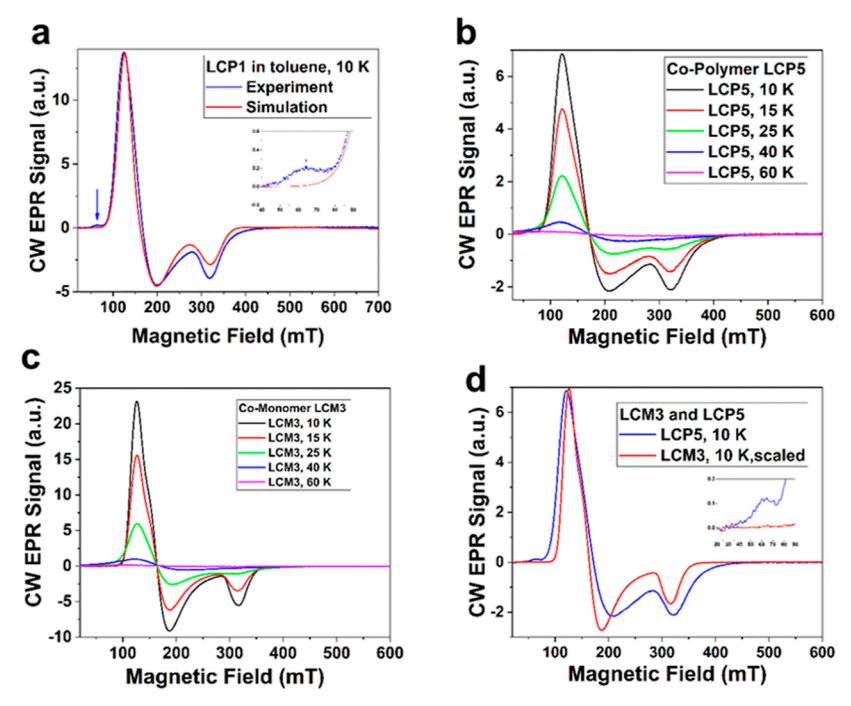


Figure 2. (a) CW X-band EPR spectrum of complex polymer LCP1 in toluene ( $\sim$ 3 mM cobalt) at low temperature (T=10 K). Note the spectral feature around  $g\approx 10-12$  indicated by an arrow, with an enlarged segment as the inset. (b) CW X-band EPR spectra of Co-polymer LCP5 in toluene ( $\sim$ 1 mg/mL cobalt) at various temperatures (10-60 K). (c) CW X-band EPR spectra of Co-monomer LCM3 in toluene ( $\sim$ 1 mM cobalt) at various temperatures (10-60 K). (d) Comparison of CW X-band EPR spectra of Co-monomer LCM3 and Co-polymer LCP5 in toluene (both  $\sim$ 1 mM cobalt) at T=10.

the neighboring magnetic center, which is likely the origin of the magnetic exchange interaction of neighboring metal centers. LCP1 exhibited molecular weight  $(M_{\rm w})$  and D of 9.5 kg/mol and 1.26, respectively, as determined by gel permeation chromatography (GPC) using polystyrene standard and CHCl<sub>3</sub> as the eluent. The thermal properties of the copolymers were determined by thermogravimetric analysis (TGA) under a nitrogen atmosphere at a heating rate of 10 °C/min (see Table S1). The polymer LCP1 showed good thermal stability with onset decomposition temperatures  $(T_{\rm d})$  corresponding to a 5% weight loss at 220 °C.

Mild reaction conditions, especially low temperatures, were used to ensure the stability of the complex polymers during polymerization. Stille polycondensation was catalyzed with the highly active catalyst Pd(PBu<sup>t</sup><sub>3</sub>)<sub>2</sub> at room temperature with high yields. To further study the magnetic properties, a series of copolymers LCP3, LCP4, and LCP5 were synthesized via postcoordination on a metal-free polymer LLP synthesized with the same polymerization method based on bipyridine monomer and TT monomer. In principle, polymers LCP1 and LCP5 are basically identical compositionally while synthesized through different pathways as shown in Figure 1a. Specifically speaking, LCP1 is synthesized from a precoordinated monomer LCM1 and another TT monomer TT-Tin via Stille polycondensation, while LCP5 is synthesized via a post-

coordination as above mentioned. The purpose of the postcoordination is to show that polymerization did not cause significant demetallation. Characterizations of these two polymers proved their similar structures; thus we only focus on one of them for the following property investigations.

Since the comonomer TT is well known to form narrow band gap polymers, the photophysical properties of the complex monomer LCM3, copolymer LCP1, and metal-free polymer (LLP, see structure details in Supporting Information, Scheme S1) were investigated by UV-vis spectroscopy (Figure 1b and Table 1). The complex monomer LCM3 showed an absorption around 310 nm, which corresponds to the absorption of the complex polymer LCP1, proving the existence of the complex unit in the copolymers. The absorption maxima of complex polymer LCP1 (green) exhibits a 75 nm redshift from the ligand polymer LLP (blue), which is due to metal-to-ligand charge transfer and enhanced intramolecular charge-transfer ability brought from the complex. Absorption maxima for thin films (red) was only slightly redshifted from that of solution of the complex polymer LCP1 due to weak aggregation of the polymer backbones in solid state, which was expected from the structure of the polymers, and the existence of the large metal center and ligands prevented the polymer backbones from significant aggregation.

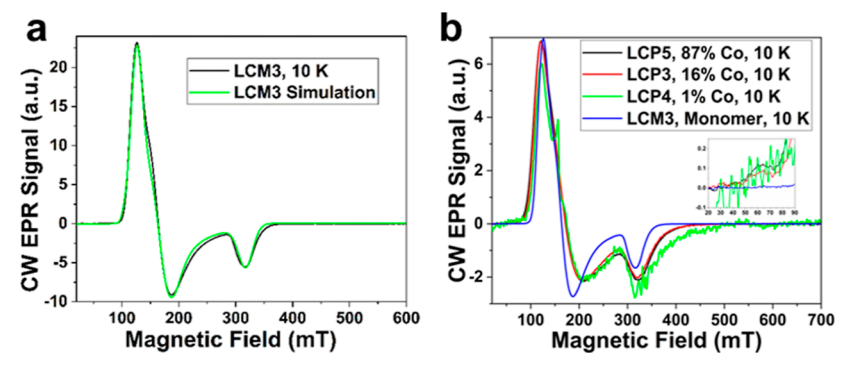


Figure 3. (a) CW X-band EPR spectrum of Co-monomer LCM3 in toluene ( $\sim$ 1 mM cobalt) at T=10 and its simulation. (b) Comparison of normalized CW X-band EPR spectra of Co-monomer LCM3 and the three copolymer samples with different ratios of Co/Zn. All samples in toluene ( $\sim$ 1 mg/mL) at T=10.

Electrochemical behavior of the polymer LCP1 was investigated by cyclic voltammetry (CV). The CV curve and their corresponding data (Figure 1c and Table 1) indicate that the onset oxidation potential ( $E_{\rm ox}$ ) was found to be 0.67 for LCP1 corresponding to the HOMO energy level of -5.00 eV. The LUMO energy level of LCP1 was estimated to be -3.62 eV, indicating a low band gap of 1.38 eV. The optical band gap was calculated from their film absorption to be 1.85 eV, which corresponds to  $\pi$ - $\pi$ \* transition. The relatively low first oxidation potential is likely due to the Co<sup>2+</sup> ions, which are known to exhibit high redox activity. A relatively wider band gap 2.40 eV was observed for the ligand polymer LLP (Figure S2), and the corresponding energy levels are summarized in Table 1.

Continuous Wave X-Band EPR Measurements. The EPR measurements were performed with a complex polymer LCP1 solution (in toluene) of approximately 3 mM cobalt content at different temperatures and with different microwave powers. The results indicated that Co(II) is a fast relaxing high-spin species. The spectrum resembles typical isolated (magnetically diluted) cobalt complexes, suggesting that the magnetic interaction (exchange and dipolar coupling) between neighboring Co(II) sites is weak relative to the linewidth. The presence of a low field signal around  $g \approx 10-12$  (indicated by an arrow in Figure 2a) is not reproduced by the simulation of isolated Co(II) species. We attribute this signal to several highspin Co(II) ions coupled with each other, yielding, for example, S = 3 or S = 9/2 species from two or three coupled Co(II) ions, respectively. Simulation of these high-spin states always produce intense peak around  $g \sim 10-12$ .

To further study the above hypothesis and investigate the effect of concentration of magnetic centers, we have designed and synthesized more polymers with varied magnetic centers (cobalt) by mixing with the corresponding diamagnetic zinc complex (see Table S1 in the Supporting Information). The complex monomer unit LCM3 was also investigated to distinguish the intermolecular interaction and intramolecular interaction. The contents of the metals in the resulting polymers were determined with ICP-MS.

Figure 2b shows the spectra of LCP5 (complex polymer with only  $Co^{2+}$  loading, similar to LCP1) at various temperatures. The spectrum at 10 K is very similar to the one of the previous polymer LCP1, which we assigned to a fast relaxing high-spin Co(II) species ( $d^7$  configuration, S = 3/2). The presence of a weak low-field signal around g = 10-12 in the spectrum of the polymer LCP1 was reproduced with the polymer LCP5.

Figure 2c shows the spectra of LCM3 (Co-monomer) at various temperatures. The general shape of the spectrum at 10 K resembles that of the Co-polymer LCP5, indicating that the electronic structure of the cobalt ion in the monomer is similar to the polymer. The temperature dependence is also similar to that of the polymer LCP5. This demonstrates that the same spin relaxation mechanisms are dominant and that the presence of cobalt ions separated by more than 10 Å is not effective in enhancing the spin relaxation rates.

A direct comparison of copolymer LCP5 and monomer LCM3 is shown for 10 K in Figure 2d. An obvious difference in the spectra is the linewidth; the signals of the monomer LCM3 are narrower by about 13 mT for the low-field signal  $(g_{\rm eff} \approx 5-6)$  and about 24 mT for the high-field signal  $(g_{\rm eff} \approx$ 2) than polymer LCP5. To make any useful comparison, we assume that the electronic and geometric structure of the cobalt centers (including ligand distances and bond lengths, and potential strain/distribution of those) is identical between LCP5 and LCM3, and thus the EPR spectrum of the polymer with only sparsely occupied binding sites would be identical to the one of the monomers LCM3. In this case, the broadening of the EPR lines can be caused either by electron spin-spin dipole interactions or exchange interactions.<sup>34</sup> If spin dipolar interaction alone were responsible for the observed broadening of the lines, the distance between neighboring cobalt centers in the polymer must be below 10 Å. However, according to DFT calculations, the distance between neighboring cobalt ions within one polymer is 12.9 Å (see Supporting Information Figure S2). The straightforward conclusion is that the broadening observed in the copolymer LCP5 with respect to LCM3 is most likely caused by the exchange interaction.

Another important difference is the absence of the low-field signal around  $g \sim 10-12$  in the LCM3 monomer spectrum (Figure 3a). This strongly supports that the  $g \sim 10-12$  signal is due to several high-spin Co(II) ions coupled with each other [two or three coupled Co(II) ions], yielding, for example, S=3 or a S=9/2 species, respectively. The interacting cobalt ions could be neighboring intrachain cobalt ions in the polymer chain or interchain aggregates. DFT calculations (Figure S3) indicate that the polymer backbone is rigid and relatively linear, meaning a folding polymer chain is unlikely. The intramolecular coupling through aggregates is thus excluded. Thus, the signal with the  $g \sim 10-12$  in LCP1 and LCP5 can be either due to the intrachain exchange coupling or interchain coupling with Co in a neighboring polymer.

To clarify the nature of the interaction signal, polymers with diluted magnetic centers were synthesized (LCP3-16% Co,

67% Zn and LCP4-1% Co, 83% Zn). EPR spectra, as shown in Figure 3b, show that the  $g \sim 10-12$  signal is significantly diminished in both samples, supporting the intrachain character of exchange coupling in LCP1 and LCP5. Besides the  $g \sim 10-12$  signal, the three polymer signals are more similar to each other than to monomer LCM3, further indicating that the broadening of the EPR lines is due to the intrachain exchange interaction. The conjugated donor–acceptor backbone behaves as a coupling unit linking the neighboring metal centers (Co-complex). The intrachain charge polarization from the D–A system enhanced the spin exchange interaction, though the physical distance is relatively large. <sup>35</sup>

Solid-State Varied-Temperature Magnetic Susceptibility. Variable-temperature DC magnetic susceptibility data were collected for the solid sample under an applied field of 10 000 Oe. The resulting plot of  $\chi_T$  versus T is shown in Figure 4.

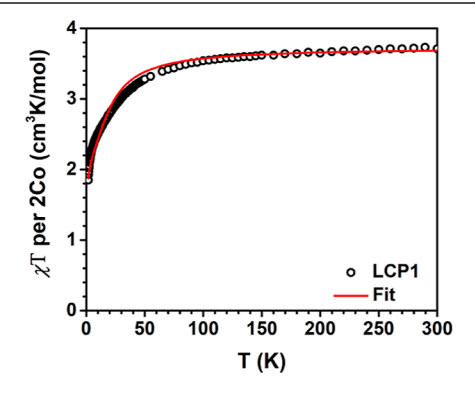


**Figure 4.** Varied-temperature of  $\chi_{\rm T}$  data for **LCP1** per two neighboring units collected under an applied field of 10 000 Oe from 300 to 1.8 K. Red line is the fit to the isotropic Heisenberg model.

At 300 K, the saturated  $\chi_T$  is about 1.86 cm<sup>3</sup> K/mol per unit corresponding to magnetically isolated high-spin Co(II) centers with g = 2.44(7). The gradual decrease of  $\chi_T$  over cooling is mainly due to the weak antiferromagnetic superexchange coupling between neighboring Co centers. The following abrupt drop, especially below 50 K, is ascribed to mainly zero-field splitting (ZFS) caused by magnetic anisotropy and antiferromagnetic coupling. To quantify the antiferromagnetic interaction, applied on two neighboring Co centers, the data were fit to the Van Vleck equation according to the spin Hamiltonian  $\hat{H} = -2J(\hat{S}_{\text{Col}},\hat{S}_{\text{Co2}})$  to give an exchange constant of J = -0.5(1.3) cm<sup>-1.36</sup> Using DAVE 2.5 program, the magnetic anisotropy is assessed with the parameter of D = -16(7) cm<sup>-1</sup>, which is obtained by fitting data with the ZFS Hamiltonian:  $\hat{H} = D\hat{S}_z^2 + g_{iso}\mu_B \mathbf{S} \cdot \mathbf{H}_{i}^{37}$  as shown in Figure 4. The observed antiferromagnetic coupling interaction is in agreement with the results from EPR measurements.

Since the exchange constant is relatively weak, the main contribution of the magnetic susceptibility is probably due to the high spin state of Co. To clarify the contribution of the D—A polymer backbone, we compared the magnetic susceptibility of the polymers LCP1 and LCM3 as shown in Figure S4. The slight difference between the two materials was caused by the D—A polymer backbone. D—A structures exhibit radical character because of the intramolecular charge polarization,<sup>24</sup> and the radical character on the coupling unit (in our case is

the D–A polymer backbone) will enhance the spin coupling effect through the direct exchange interaction. <sup>18,19</sup> For the ligand polymer **LLP**, the donor–acceptor effect is relatively weak which can be seen from its CV measurement (Figure S2), corresponding to a relatively wide band gap of 2.40 eV. This is consistent with a relative weak exchange constant between the neighboring Co ions.

**Faraday Effect.** The MOA of LCP1 was characterized using magnetic circular dichroism (MCD) spectroscopy (Figure 5). The magneto-optic rotary dispersion (MORD)

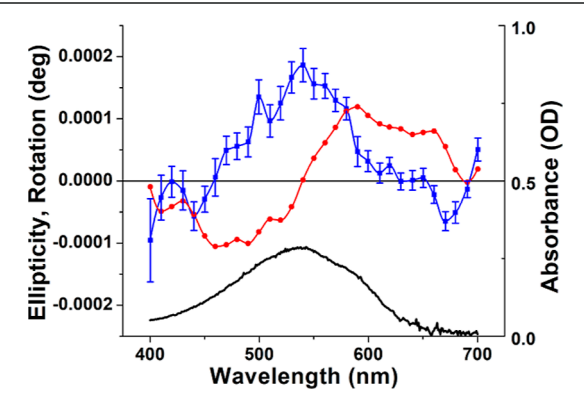


**Figure 5.** MCD spectrum of **LCP1** thin film (blue), MORD spectrum estimated by numerical Kramers–Kronig analysis (red), and a representative absorbance spectrum of an **LCP1** thin film (black). Applied field was 0.4 T.

spectrum, also known as Faraday rotation spectroscopy, was estimated using the Kramers-Kronig transform.<sup>38-40</sup> The MCD spectrum (blue trace) follows the absorbance spectra closely, and the peak of the dichroism is centered at the peak of the absorbance spectra. This correlation between the MCD and UV-visible absorption spectrum implies that the MOA signal arises from Faraday B- and C-terms.<sup>41</sup> The calculated MORD roughly follows the first Gaussian derivative line-shape (red trace). Faraday B-terms correspond to magnetic fieldinduced excited-state mixing with the states involved in the electronic transition, while C-terms correspond to the magnetic field-induced splitting of paramagnetic ground states.42 These results are consistent with the presence of paramagnetic cobalt ions in the polymer, which are known to exhibit magneto-optic C-terms.<sup>43</sup> Faraday C-terms are typically more intense than B-terms. 42 Given the very short path-length of the magneto-optically active material, ~100 nm, the material exhibits a large magneto-optic rotation with a peak Verdet constant of 2980 deg·T<sup>-1</sup>·m<sup>-1</sup> at 590 nm. For comparison, terbium gallium garnet, an industrially relevant magneto-optic crystal, has a Verdet constant of 7505 deg·T<sup>-1</sup>·m<sup>-1</sup> at 632 nm. 44 The high Verdet constant demonstrates the potential of this hybrid material for the development of new magnetooptically active thin-film polarization control materials and devices. By incorporating a metal ion directly into the polymer backbone, the thin film is rendered magneto-optically active, and a new synthetic handle is introduced to study a range of interesting magnetic and magneto-optic effects through substitution of the metal center.

We note that the Verdet constant reported here is roughly an order of magnitude less than what we observed for similar polymers, which do not contain a transition metal center. <sup>45</sup> Of particular interest is that those P3HT-based materials only exhibited a B-term or magnetic field-induced excited-state

coupling contribution to the overall MOA of the material, whereas these present films also contain paramagnetic metal centers. By virtue of their unpaired electrons, paramagnetic metal centers contribute an intense C-term to the MOA, and yet these composite materials are less magneto-optically active. It thus appears as if the terms are acting in opposition with one another. While the exact origin of this effect is under investigation, we speculate that a disordered morphology may conspire to minimize the MOA. Last, we acknowledge that the MOA is ultimately a response to the absorptivity of the film, regardless of the thickness.

## CONCLUSIONS

In conclusion, we have developed a donor-acceptor Cocontaining conjugated complex polymer. This polymer was synthesized via Stille coupling reactions under mild conditions, and the Co-complex remains intact. The optical and electrochemical properties show it being a narrow band gap material. SQUID and CW X-band EPR measurements of the complex polymer and two corresponding reference polymers showed that there is an intrachain exchange interaction between the neighboring metal centers. The key reason for this property is that the donor-acceptor interaction caused intrachain charge polarization along the polymer backbone. As a coupling unit, the partially charged polymer backbone enhanced the super-exchange interactions between magnetic centers. A high Verdet constant was observed by Faraday rotation spectroscopy, demonstrating the potential of this hybrid material as new magneto-optically active thin-film materials for polarization control. This work provides an effective and promising approach for synthesizing conjugated (anti)ferromagnetic polymers.

# **■ EXPERIMENTAL SECTION**

<sup>1</sup>H NMR was recorded on a Bruker DRX-500 spectrometer. MALDI-TOF mass spectra were recorded using a Bruker UltrafleXtreme MALDI-TOF mass spectrometer. Ultraviolet-visible-near IR (UVvis-NIR) spectra of the monomers and polymers were measured on a SHIMADZU UV-3600 spectrometer. The elemental analyses of the polymers were performed on an Elementar Vario EL III element analyzer for C, H, F, N, and S determination. TGAs were performed under nitrogen at a heating rate of 10 °C/min using a SHIMADZU TGA-50 analyzer. The average molecular weight and polydispersity index (D) of the polymers were determined using Waters 1515 GPC analysis with CHCl<sub>3</sub> as the eluent and polystyrene as the standard. There are two detectors for the instrument, refractive index detector and UV-vis detector. In this study, all molecular weight is collected from the traces with the UV-vis detector. Electrochemical redox potentials were obtained by CV using a three-electrode configuration and an electrochemistry workstation (AUTOLAB PGSTAT12). CV was conducted on an electrochemistry workstation with the polymer thin film on a Pt working electrode, Pt as the counter electrode as well, and Ag/AgCl as the reference electrode in a 0.1 M tetra-nbutylammonium hexafluorophosphate acetonitrile solution at a scan rate of 50 mV/s. The redox potentials were first referenced to the ferrocene/ferrocenium redox couple (Fc/Fc<sup>+</sup>) which is at 0.47 V versus SCE. The redox potential of Fc/Fc<sup>+</sup> was then assumed to be at -4.8 eV relative to vacuum. 46 Then HOMO/LUMO energy levels and electrochemical energy gaps  $(E_{\rm g}^{\rm \ ec})$  of our copolymers were calculated as per the following equations

HOMO = 
$$-(E_{ox} + 4.33)$$
 (eV)  
LUMO =  $-(E_{red} + 4.33)$  (eV)  
 $E_{\sigma}^{ec} = (E_{ox} - E_{red})$  (eV)

ICP-MS data were obtained with an Agilent 7700x ICP-MS spectrometer and analyzed using ICP-MS Mass Hunter version B01.03. A commercially available standard E2-TB01060 from the company Inorganic Ventures was used. The vacuum dried sample (10 mg) was weighed in a glass vial. Metal-free, 70% nitric acid (1 mL) was added to each vial and then incubated in a 80 °C water bath for 3 h until all solid samples were dissolved. The digested sample in 70% nitric acid was diluted 35 times by DI water to prepare a 2% nitric acid solution and then further diluted by 2% nitric acid until the ICP-MS read out below 500 ppb.

Faraday rotation was detected using a homodyne detection scheme. A 532 nm diode laser was initially polarized at 45°. This light was directed through a thin-film sample mounted in the center of a solenoid. The reference frequency generated by a Stanford research instruments SR830 lock-in amplifier was further amplified and used to generate a low-frequency magnetic field.

CW X-band (9–10 GHz) EPR experiments were carried out with a Bruker ELEXSYS II E500 EPR spectrometer (Bruker BioSpin, Rheinstetten, Germany) equipped with a TE<sub>102</sub> rectangular EPR resonator (Bruker ER 4102ST). Field modulation at 100 kHz in combination with lock-in detection leads to first derivative-type CW EPR spectra. Measurements were performed at cryogenic temperatures. A helium gas-flow cryostat (ICE Oxford, UK) and an ITC (Oxford Instruments, UK) were used for temperature control. Data processing was performed using Xepr (Bruker BioSpin, Rheinstetten, Germany) and spectral simulations using the EasySpin program package<sup>47</sup> in MATLAB R2018b (MathWorks, Natick) environment.

Solid-state magnetic measurement was carried out with a MPMS-XL Quantum Design SQUID operating at temperatures between 1.8 and 300 K at 1 T DC magnetic field. Measurements was performed on a powder sample of LCP1 (24.1 mg) mixed with eicosane (18.0 mg) in a plastic capsule (34.3 mg). DC susceptibility data were corrected for the intrinsic diamagnetic contributions of the sample and those from the sample holder and fixer.

MCD spectra were collected on a spectrometer built in-house (Figure 6), incorporating a 150 W Xe-arc lamp source, a Spectral

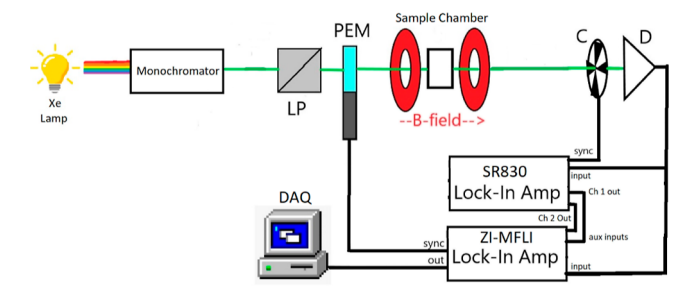


**Figure 6.** Block diagram of the MCD spectrometer. Focusing and collimating optics occluded for clarity. LP = linear polarizer, PEM = photo-elastic modulator, C = chopper, and D = detector.

Products CM110 monochromator, a Hinds Instruments PEM-100 photoelastic modulator (50 kHz operating frequency), a Terahertz Technologies C-995 optical chopper, and a Thorlabs DET300A detector. Field was applied using a lab-built magnetized sample chamber which generated 0.4 T along or against the optical axis of the spectrometer. Signal demodulation and measurement were accomplished using a Stanford research instruments SR-830 and a Zurich Instruments ZI-MFLI lock-in amplifiers with data acquisition executed *via* LabView. Field was reversed between paired experiments to ensure validity of the magneto-optic spectra. An instrument block diagram is depicted in Figure S1. Kramers—Kronig analysis was performed in MATLAB using a program based on published MATLAB code. 40,50,51

#### ASSOCIATED CONTENT

## **5** Supporting Information

The Supporting Information is available free of charge at https://pubs.acs.org/doi/10.1021/acs.chemmater.2c01433.

Detailed syntheses of the monomers and polymers and DFT calculation results of copolymers (PDF)

#### AUTHOR INFORMATION

#### **Corresponding Authors**

Xunshan Liu — Key Laboratory of Surface & Interface Science of Polymer Materials of Zhejiang Province, Department of Chemistry, Zhejiang Sci-Tech University, Hangzhou 310018, China; Department of Chemistry and the James Franck Institute, The University of Chicago, Chicago, Illinois 60637, United States; orcid.org/0000-0003-1537-258X; Email: xliu350@zstu.edu.cn

Luping Yu — Department of Chemistry and the James Franck Institute, The University of Chicago, Chicago, Illinois 60637, United States; Email: lupingyu@uchicago.edu

#### **Authors**

Jiaze Xie − Department of Chemistry and the James Franck Institute, The University of Chicago, Chicago, Illinois 60637, United States; ② orcid.org/0000-0003-1813-9521

Jens Niklas − Chemical Sciences and Engineering Division, Argonne National Laboratory, Lemont, Illinois 60439, United States; © orcid.org/0000-0002-6462-2680

Emigdio E. Turner – Laboratory for Magneto-Optical Spectroscopy, Department of Chemistry and Chemical Biology, University of New Mexico, Albuquerque, New Mexico 87131, United States

Dafei Yuan — Department of Chemistry and the James Franck Institute, The University of Chicago, Chicago, Illinois 60637, United States; orcid.org/0000-0001-5914-2060

John S. Anderson – Department of Chemistry and the James Franck Institute, The University of Chicago, Chicago, Illinois 60637, United States; orcid.org/0000-0002-0730-3018

Jeffrey J. Rack – Laboratory for Magneto-Optical Spectroscopy, Department of Chemistry and Chemical Biology, University of New Mexico, Albuquerque, New Mexico 87131, United States; orcid.org/0000-0001-6121-879X

Oleg G. Poluektov — Chemical Sciences and Engineering Division, Argonne National Laboratory, Lemont, Illinois 60439, United States; oorcid.org/0000-0003-3067-9272

Complete contact information is available at: https://pubs.acs.org/10.1021/acs.chemmater.2c01433

## **Author Contributions**

<sup>1</sup>X.L. and J.X. contributed equally.

#### **Notes**

The authors declare no competing financial interest.

#### ACKNOWLEDGMENTS

This work was supported by the Natural Science Foundation of Zhejiang Province (LQ22B040003), the National Natural Science Foundation of China (22105172), the Fundamental Research Funds of Zhejiang Sci-Tech University (21062113-Y), and the NSF (CHE-2102102, L.Y.). J.S.A. gratefully acknowledges the National Science Foundation (DMR-2002367), the Sloan Research Foundation (FG-2019-11497), and 3M Corporation through an NTFA. J.J.R. (UNM)

acknowledges the financial support of thebNSF (CHE 1856492). The EPR work at Argonne National Laboratory (J.N., O.G.P.) was supported by the U.S. Department of Energy (DOE), Office of Basic Energy Sciences, Division of Chemical Sciences, Geosciences, and Biosciences under contract no. DE-AC-02-06CH11357. We thank Xiaomin Jiang for the ICP-MS measurements.

#### ■ REFERENCES

- (1) Dou, L.; Gao, J.; Richard, E.; You, J.; Chen, C.-C.; Cha, K. C.; He, Y.; Li, G.; Yang, Y. Systematic Investigation of Benzodithiophene-and Diketopyrrolopyrrole-Based Low-Bandgap Polymers Designed for Single Junction and Tandem Polymer Solar Cells. *J. Am. Chem. Soc.* **2012**, *134*, 10071–10079.
- (2) Carsten, B.; He, F.; Son, H. J.; Xu, T.; Yu, L. Stille Polycondensation for Synthesis of Functional Materials. *Chem. Rev.* **2011**, *111*, 1493–1528.
- (3) Xu, J.; Wang, S.; Wang, G.-J. N.; Zhu, C.; Luo, S.; Jin, L.; Gu, X.; Chen, S.; Feig, V. R.; To, J. W. F.; Rondeau-Gagné, S.; Park, J.; Schroeder, B. C.; Lu, C.; Oh, J. Y.; Wang, Y.; Kim, Y.-H.; Yan, H.; Sinclair, R.; Zhou, D.; Xue, G.; Murmann, B.; Linder, C.; Cai, W.; Tok, J. B.-H.; Chung, J. W.; Bao, Z. Highly Stretchable Polymer Semiconductor Films through the Nanoconfinement Effect. *Science* 2017, 355, 59.
- (4) Kawamura, A.; Xie, J.; Boyn, J.-N.; Jesse, K. A.; McNeece, A. J.; Hill, E. A.; Collins, K. A.; Valdez-Moreira, J. A.; Filatov, A. S.; Kurutz, J. W.; Mazziotti, D. A.; Anderson, J. S. Reversible Switching of Organic Diradical Character via Iron-Based Spin-Crossover. *J. Am. Chem. Soc.* **2020**, 142, 17670–17680.
- (5) Senthil Kumar, K.; Ruben, M. Emerging Trends in Spin Crossover (SCO) Based Functional Materials and Devices. *Coord. Chem. Rev.* **2017**, 346, 176–205.
- (6) Kipgen, L.; Bernien, M.; Tuczek, F.; Kuch, W. Spin-Crossover Molecules on Surfaces: From Isolated Molecules to Ultrathin Films. *Adv. Mater.* **2021**, 33, No. e2008141.
- (7) Coronado, E. Molecular Magnetism: from Chemical Design to Spin Control in Molecules, Materials and Devices. *Nat. Rev. Mater.* **2020**, *5*, 87–104.
- (8) Woodruff, D. N.; Winpenny, R. E. P.; Layfield, R. A. Lanthanide Single-Molecule Magnets. *Chem. Rev.* **2013**, *113*, 5110–5148.
- (9) Wilson, J. S.; Dhoot, A. S.; Seeley, A. J. A. B.; Khan, M. S.; Köhler, A.; Friend, R. H. Spin-Dependent Exciton Formation in  $\pi$ -conjugated Compounds. *Nature* **2001**, *413*, 828–831.
- (10) Peng, Z.; Yu, L. Synthesis of Conjugated Polymers Containing Ionic Transition Metal Complexes. *J. Am. Chem. Soc.* **1996**, *118*, 3777–3778.
- (11) Wang, Q.; Yu, L. Conjugated Polymers Containing Mixed-Ligand Ruthenium (II) Complexes. Synthesis, Characterization, and Investigation of Photoconductive Properties. *J. Am. Chem. Soc.* **2000**, *122*, 11806–11811.
- (12) Yuan, S.; Jaramillo, R.; Rosenbaum, T. F.; Yu, L. Synthesis and Characterization of Conjugated Polymers Containing First Row Transition Metal Complexes. *Macromolecules* **2006**, *39*, 8652–8658.
- (13) Ni, Y.; Gopalakrishna, T. Y.; Wu, S.; Wu, J. A Stable All-Thiophene-Based Core-Modified [38]Octaphyrin Diradicaloid: Conformation and Aromaticity Switch at Different Oxidation States. *Angew. Chem., Int. Ed.* **2020**, *59*, 7414–7418.
- (14) Gallagher, N.; Zhang, H.; Junghoefer, T.; Giangrisostomi, E.; Ovsyannikov, R.; Pink, M.; Rajca, S.; Casu, M. B.; Rajca, A. Thermally and Magnetically Robust Triplet Ground State Diradical. *J. Am. Chem. Soc.* 2019, 141, 4764–4774.
- (15) Meng, Y.-S.; Sato, O.; Liu, T. Manipulating Metal-to-Metal Charge Transfer for Materials with Switchable Functionality. *Angew. Chem., Int. Ed.* **2018**, *57*, 12216–12226.
- (16) Wei, R. M.; Liu, T.; Li, J.; Zhang, X.; Chen, Y.; Zhang, Y. Q. Tuning the Magnetization Dynamic Properties of Nd···Fe and Nd··· Co Single-Molecular Magnets by Introducing 3 d–4 f Magnetic Interactions. *Chem.—Asian J.* **2019**, *14*, 2029–2035.

- (17) Chen, Y.; Ma, F.; Chen, X.; Dong, B.; Wang, K.; Jiang, S.; Wang, C.; Chen, X.; Qi, D.; Sun, H.; Wang, B.; Gao, S.; Jiang, J. A New Bis(phthalocyaninato) Terbium Single-Ion Magnet with an Overall Excellent Magnetic Performance. *Inorg. Chem.* **2017**, *56*, 13889–13896.
- (18) Boyn, J.-N.; Xie, J.; Anderson, J. S.; Mazziotti, D. A. Entangled Electrons Drive a Non-Superexchange Mechanism in a Cobalt Quinoid Dimer Complex. *J. Phys. Chem. Lett.* **2020**, *11*, 4584–4590.
- (19) Demir, S.; Jeon, I.-R.; Long, J. R.; Harris, T. D. Radical Ligand-containing Single-Molecule Magnets. *Coord. Chem. Rev.* **2015**, 289–290, 149–176.
- (20) Barker, J. E.; Dressler, J. J.; Valdivia, A. C.; Kishi, R.; Strand, E. T. Molecule Isomerism Modulates the Diradical Properties of Stable Singlet Diradicaloids. *J. Am. Chem. Soc.* **2020**, *142*, 1548–1555.
- (21) Chen, C.; Ruan, H.; Feng, Z.; Fang, Y.; Tang, S.; Zhao, Y.; Tan, G.; Su, Y.; Wang, X. Crystalline Diradical Dianions of Pyrene-Fused Azaacenes. *Angew. Chem., Int. Ed.* **2020**, *59*, 11794–11799.
- (22) Feng, Y.; Zhang, F.; Song, X.; Bu, Y. Molecular Vibrations Induced Potential Diradical Character in Hexazapentacene. *J. Phys. Chem. C* **2016**, *120*, 10215–10226.
- (23) Degayner, J. A.; Jeon, I.-R.; Sun, L.; Dincă, M.; Harris, T. D. 2D Conductive Iron-Quinoid Magnets Ordering up to Tc = 105 K via Heterogenous Redox Chemistry. *J. Am. Chem. Soc.* **2017**, *139*, 4175–4184.
- (24) Chen, Z.; Li, W.; Sabuj, M. A.; Li, Y.; Zhu, W.; Zeng, M.; Sarap, C. S.; Huda, M. M.; Qiao, X.; Peng, X.; Ma, D.; Ma, Y.; Rai, N.; Huang, F. Evolution of The Electronic Structure in Open-Shell Donor-Acceptor Organic Semiconductors. *Nat. Commun.* 2021, 12, 5889.
- (25) Peng, Z.; Gharavi, A. R.; Yu, L. Synthesis and Char acterization of Photorefractive Polymers Containing Transition Metal Complexes as Photosensitizer. *J. Am. Chem. Soc.* **1997**, *119*, 4622–4632.
- (26) Peng, Z.; Yu, L. Synthesis of Conjugated Polymers Containing Ionic Transition Metal Complexes. *J. Am. Chem. Soc.* **1996**, *118*, 3777–3778.
- (27) Wang, Q.; Yu, L. Conjugated Polymers Containing Mixed-Ligand Ruthenium (II) Complexes. Synthesis, Characterization, and Investigation of Photoconductive Properties. *J. Am. Chem. Soc.* **2000**, 122, 11806–11811.
- (28) Yuan, S.; Jaramillo, R.; Rosenbaum, T. F.; Yu, L. Synthesis and Characterization of Conjugated Polymers Containing First Row Transition Metal Complexes. *Macromolecules* **2006**, *39*, 8652–8658.
- (29) Liu, F.; Espejo, G. L.; Qiu, S.; Oliva, M. M.; Pina, J.; Seixas de Melo, J. S.; Casado, J.; Zhu, X. Multifaceted Regioregular Oligo-(thieno[3,4-b]thiophene)s Enabled by Tunable Quinoidization and Reduced Energy Band Gap. J. Am. Chem. Soc. 2015, 137, 10357—10366.
- (30) Liu, X.; Sharapov, V.; Zhang, Z.; Wiser, F.; Awais, M. A.; Yu, L. Photoinduced Cationic Polycondensation in Solid State Towards Ultralow Band Gap Conjugated Polymers. *J. Mater. Chem. C* **2020**, *8*, 7026–7033
- (31) Díaz, J. F.; Balkus, K. J.; Bedioui, F.; Kurshev, V.; Kevan, L. Synthesis and Characterization of Cobalt Complex Functionalized MCM-41. *Chem. Mater.* **1997**, *9*, 61–67.
- (32) Wasylenko, D. J.; Ganesamoorthy, C.; Borau-Garcia, J.; Berlinguette, C. P. Electrochemical Evidence for Catalytic Water Oxidation Mediated by a High-valent Cobalt Complex. *Chem. Commun.* **2011**, 47, 4249.
- (33) Chujo, Y.; Sada, K.; Saegusa, T. Cobalt (III) Bipyridyl-Branched Polyoxazoline Complex as a Thermally and Redox Reversible Hydrogel. *Macromolecules* **1993**, *26*, 6320–6323.
- (34) Carrington, A.; Mclachlan, D. A. Introduction to Magnetic Resonance: with Applications to Chemistry and Chemical Physics, 2nd ed.; Harper & Row: New York, 1969; p 566.
- (35) Coffman, R. E.; Buettner, G. R. A Limit Function for Long-Range Ferromagnetic and Antiferromagnetic Superexchange. *J. Phys. Chem.* 1979, 83, 2387–2392.
- (36) Boča, R. Theoretical Foundations of Molecular Magnetism; Elsevier: Amsterdam, 1999; pp 313-344.

- (37) Azuah, R. T.; Kneller, L. R.; Qiu, Y.; Tregenna-Piggott, P. L. W.; Brown, C. M.; Copley, J. R. D.; Dimeo, R. M. DAVE: A Comprehensive Software Suite for the Reduction, Visualization, and Analysis of Low Energy Neutron Spectroscopic Data. *J. Res. Natl. Inst. Stand. Technol.* **2009**, 114, 341–358.
- (38) Shackleford, W. L.; Penner, S. S. Erratum: Ionization Mechanism of Chromium in Cr-Ar Mixtures. *J. Chem. Phys.* **1968**, 49. 1448.
- (39) Polavarapu, P. L. Kramers-Kronig Transformation for Optical Rotatory Dispersion Studies. *J. Phys. Chem. A* **2005**, *109*, 7013–7023. (40) Healy, W. P.; Power, E. A. Dispersion Relations for Optically Active Me dia. *Am. J. Phys.* **1974**, *42*, 1070–1074.
- (41) Buckingham, A. D.; Stephens, P. J. Magnetic Optical Activity. *Annu. Rev. Phys. Chem.* **1966**, *17*, 399–432.
- (42) Barron, L. D. Molecular Light Scattering and Optical Activity, 2nd ed.; University Press: Cambridge, 2004; pp 311–330.
- (43) Shashoua, V. E. General Characteristics of Magneto-Opti cal Rotation Spectra. J. Am. Chem. Soc. 2002, 86, 2109–2115.
- (44) Vojna, D.; Slezák, O.; Lucianetti, A.; Mocek, T. Verdet Constant of Magneto-Active Materials Developed for High-Power Faraday Devices. *Appl. Sci.* **2019**, *9*, 3160.
- (45) Liu, X.; Turner, E. E.; Sharapov, V.; Yuan, D.; Awais, M. A.; Rack, J. J.; Yu, L. Finely Designed P3HT-Based Fully Conjugated Graft Polymer: Optical Measurements, Morphology, and the Faraday Effect. ACS Appl. Mater. Interfaces 2020, 12, 30856–30861.
- (46) Wang, M.; Hu, X.; Liu, P.; Li, W.; Gong, X.; Huang, F.; Cao, Y. Donor—Acceptor Conjugated Polymer Based on Naphtho[1,2-c:5,6-c]bis[1,2,5]thiadiazole for High-Performance Polymer Solar Cells. J. Am. Chem. Soc. 2011, 133, 9638—9641.
- (47) Stoll, S.; Schweiger, A. EasySpin, A Comprehensive Software Package for Spectral Simulation and Analysis In EPR. *J. Magn. Reson.* **2006**, *178*, 42–55.
- (48) Hipps, K. W.; Crosby, G. A. Applications of the Photoe lastic Modulator to Polarization Spectroscopy. *J. Phys. Chem.* **1979**, *83*, 555–562.
- (49) Drake, A. F. Polarisation Modulation-the measurement of Linear and Circular Dichroism. *J. Phys. E: Sci. Instrum.* **1986**, *19*, 170–181.
- (50) Lucarini, V.; Saarinen, J.; Peiponen, K. E.; Vartiainen, E. Kramers-Kronig Relations in Optical Materials Research; Springer Berlin Heidelberg, 2005.
- (51) Emeis, C. A.; Oosterhoff, L. J.; Vries, G. D. Numerical Evaluation of Kramers-Kronig Relations. *Proc. R. Soc. London, Ser. A* **1967**, 297, 54–65.